nature neuroscience

Melanin-concentrating hormone regulates beat frequency of ependymal cilia and ventricular volume

Grégory Conductier[1,2,10], Frédéric Brau[1,2,10], Angèle Viola[3,10], Fanny Langlet[4], Navean Ramkumar[2,5], Bénédicte Dehouck[4], Thibault Lemaire[1,2], Raphaël Chapot[1,2], Laurianne Lucas[1,2], Carole Rovère[1,2], Priscilla Maitre[1,2], Salma Hosseiny[1,2], Agnès Petit-Paitel[1,2], Antoine Adamantidis[6], Bernard Lakaye[7], Pierre-Yves Risold[8], Vincent Prévot[4,11], Olivier Meste[2,5,11], Jean-Louis Nahon[1,2,9,11] & Alice Guyon[1,2,11]

Ependymal cell cilia help move cerebrospinal fluid through the cerebral ventricles, but the regulation of their beat frequency remains unclear. Using *in vitro*, high-speed video microscopy and *in vivo* magnetic resonance imaging in mice, we found that the metabolic peptide melanin-concentrating hormone (MCH) positively controlled cilia beat frequency, specifically in the ventral third ventricle, whereas a lack of MCH receptor provoked a ventricular size increase.

The wall of the cerebral ventricles, which separates the cerebrospinal fluid (CSF) from the brain parenchyma, mainly consists of ciliated epithelial cells whose coordinated beating facilitates CSF circulation[1]. Proper circulation of CSF is crucial for brain functioning, as defects in ventricular cilia result in hydrocephalus, owing to an excess of CSF[2]. Although numerous studies have focused on the biogenesis and orientation of cilia[3], little is known about their physiology, and the precise role of neuropeptides[4] in regulating the cilia beat frequency (CBF) remains elusive. We tested whether the hypothalamic MCH peptide modulates CSF flow through a direct action on CBF. In mammals, MCH-expressing neurons are mainly located in the lateral hypothalamic area (LHA), and send projections throughout the brain[5], consistent with MCH's large repertoire of physiological actions. In addition to synaptic transmission, MCH could also be involved in non-neuronal intercellular communication and 'volume' transmission, but evidence is lacking.

In coronal brain sections from adult *Pmch-CFP* transgenic mice, we found MCH-containing fibers surrounded the ventral part of the third ventricle (v3V; **Fig. 1a** and **Supplementary Figs. 1a–f** and **2b–d**). Indeed, few if any fibers were visible around the dorsal third ventricle (d3V), the lateral ventricles (LVs; **Supplementary Fig. 1g–j**) or in the median eminence (**Supplementary Fig. 2e**). Some of these fibers were in direct contact with the CSF (**Supplementary Fig. 1e**), where they may release MCH, as we detected the peptide in the CSF at nanomolar concentrations (**Supplementary Table 1**).

To determine the localization and nature of MCHR1-expressing epithelial cells, we performed triple immunolabeling for MCHR1, glu-tubulin and vimentin (**Fig. 1a** and **Supplementary Fig. 2**), two specific markers of cilia and ependymal cells, respectively, in hypothalamic sections from adult *Pmch-CFP* mice. MCH terminals appeared to contact ciliated ependymal cells in the v3V (**Fig. 1a**), but did not contact the median eminence or d3V (**Supplementary Fig. 2e**). Moreover, only those ciliated ependymal cells contacted by MCH fibers expressed MCHR1 (**Fig. 1a**).

We then tested whether MCH peptide regulated the CBF by developing high-speed, bright-field video microscopy imaging of brain slices (**Supplementary Movie 1** and Online Methods) and a maximum likelihood estimator for the analysis of the CBF (O.M., F.B. and A.G., http://hal.archives-ouvertes.fr/hal-00806681). To validate our model and measurement system, we bath-applied serotonin (5-HT, 50 µM) or ATP (100 µM) (**Fig. 1b–e** and **Supplementary Fig. 3a**). The two neuromodulators increased the CBF in both the v3V (5-HT: +48.5 ± 9%, $N = 4$ slices from 2 mice, $t_{(7)} = 4.148$, $P < 0.01$; ATP: +124.8 ± 42.0%, $N = 7$ slices from 3 mice, $t_{(10)} = 3.784$, $P < 0.05$) and the d3V and LVs (data not shown, $N = 6$ slices from 3 mice).

Using this setup, we found that MCH treatment (1 µM) increased the ependymal cells CBF in the v3V by 39.5 ± 5.6% ($N = 20$ slices from 5 mice, $t_{(19)} = 7.497$, $P < 0.001$; **Fig. 1b**,**c**,**e**). In contrast with 5-HT or ATP treatment, MCH treatment had no effect on the CBF recorded in the d3V ($N = 2$ slices from 2 mice, $P > 0.05$) or the LVs ($N = 4$ slices from 2 mice, $P > 0.05$), consistent with the absence of MCH-containing fibers or MCHR1 labeling in this area. MCH's effect on the CBF was concentration dependent, reaching a maximum at 1 µM with a half-maximal effect at 0.44 ± 0.03 nM (**Supplementary Fig. 3b**). Notably, this effect was completely abolished in mice lacking the *Mchr1* gene (*Mchr1*$^{-/-}$), the only functional receptor mediating MCH action in rodents[6] ($N = 22$ slices from 8 mice, $t_{(19)} = 1.348$, $P > 0.05$; **Fig. 1d**,**e** and **Supplementary Fig. 3c**), and was blocked by the MCHR1 antagonist H-6408 (250 nM; $N = 4$ slices from 2 mice, $t_{(7)} = 2.287$, $P > 0.05$; **Fig. 1d**,**e**). H-6408 significantly decreased basal CBF by 29.29 ± 5.89% in wild-type mice ($N = 17$ slices from 5 mice, $t_{(16)} = 8.318$, $P < 0.001$), suggesting that MCHR1 is tonically activated in slices (**Fig. 1d**,**e**). This effect was absent in *Mchr1*$^{-/-}$ mice ($N = 20$ slices from 7 mice, $t_{(19)} = 0.391$, $P > 0.05$; **Fig. 1e** and **Supplementary Fig. 3c**), further confirming the selectivity of this antagonist. The spontaneous CBF recorded in slices from *Mchr1*$^{-/-}$ mice was

[1]Institut de Pharmacologie Moléculaire et Cellulaire, UMR 7275 Centre National de la Recherche Scientifique (CNRS), Valbonne, France. [2]University of Nice Sophia Antipolis, Nice, France. [3]Aix-Marseille Université, Centre de Résonance Magnétique Biologique et Médicale, UMR 7339 CNRS, Faculté de Médecine la Timone, Marseille, France. [4]INSERM U837/University of Lille 2, Lille, France. [5]I3S, UMR 7271 CNRS, Sophia Antipolis, France. [6]Douglass Mental Health University Intitute, Montreal, Quebec, Canada. [7]University of Liège, GIGA-Neurosciences, Liège, Belgium. [8]Laboratoire d'Histologie, EA3922, SFR FED 4234, Faculté de Médecine et de Pharmacie, Besançon, France. [9]Station de Primatologie, UPS 846 CNRS, Rousset sur Arc, France. [10]These authors contributed equally to this work. [11]These authors jointly directed this work. Correspondence should be addressed to A.G. (alice.guyon@ipmc.cnrs.fr) or J.-L.N. (nahonjl@ipmc.cnrs.fr).

Received 9 January; accepted 18 April; published online 26 May 2013; doi:10.1038/nn.3401

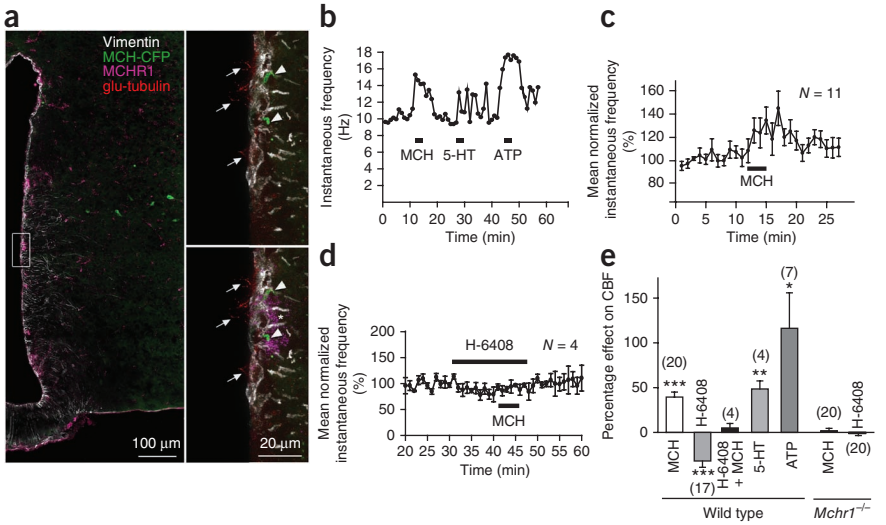

Figure 1 MCH increases ependymal cell CBF in the v3V, where MCH fibers and MCHR1 are present in close apposition. (**a**) Vimentin, glu-tubulin and MCHR1 immunoreactivity in coronal hypothalamus sections from *Pmch-CFP* mice. Insets, high-magnification images of MCH fibers (arrowheads) running close to the ependymal cell layer with cilia (arrows) and MCHR1. (**b**,**c**) Single (**b**) and normalized averaged (± s.e.m.; **c**) ependymal cell CBF responses to MCH (1 µM), 5-HT (50 µM) and ATP (100 µM) (indicated by bars). (**d**) The MCH effect on CBF was blocked by H-6408, which independently decreased the CBF. (**e**) Mean CBF peak variation (± s.e.m.) expressed as a percentage of the spontaneous CBF. Single group one-sample *t* test compared with a theoretical mean µ = 0, $^{*}P < 0.05$, $^{**}P < 0.01$, $^{***}P < 0.001$. Numbers of slices in parentheses, 1–3 slices per mouse.

significantly lower than that of wild-type mice ($Mchr1^{-/-}$, 4.97 ± 0.64 Hz, N = 23 slices from 8 mice; wild type, 11.18 ± 0.72 Hz, N = 55 slices from 14 mice; Mann-Whitney test, t = 476.5, U = 200.5, $P < 0.001$), suggesting that MCHR1 has a tonic stimulating action on CBF in the v3V.

We next studied the direct action of MCH peptide on ependymal cells using whole-cell patch-clamp recordings (**Supplementary Fig. 4**). MCH (1 µM) induced a small hyperpolarization (–18.25 ± 7.89 mV from resting potential, n = 4 cells recorded, N = 4 slices from 2 mice). In voltage clamp, the MCH-activated current had an inversion potential close to –80 mV, suggesting that it was carried by potassium ions. Bath application of 50 nM charybdotoxin, a large and intermediate-conductance calcium-activated potassium channels (BK/IK) inhibitor, decreased the current by 88% (n = 9 cells recorded, N = 9 slices from 6 mice, $t_{(8)}$ = 19.25, $P < 0.001$), suggesting that MCHR1 stimulation activates a calcium-dependent potassium channel. Indeed, we found that application of 1 µM MCH increased calcium levels in Fura-2AM–loaded ciliated cells (ΔF = 5.4 ± 1.32% relative to baseline, N = 11 slices from 5 mice, $t_{(10)}$ = 4.049, $P < 0.01$; **Supplementary Fig. 5**). This effect was blocked by H-6408 (250 nM, N = 6 slices from 3 mice, $t_{(5)}$ = 1.536, $P > 0.05$).

We further confirmed these results by electrically (voltage and current application using a bipolar electrode) or chemically (KCl 135 mM, applied from a patch pipette) stimulating LHA in brain slices while recording ipsilaterally to the stimulation. Although both types of stimuli increased the CBF, electrical stimulations were the most efficient at reliably increasing the CBF (electrical: +55.44 ± 7.78%, N = 18 slices from 5 mice, $t_{(17)}$ = 8.682, $P < 0.001$; chemical: +24.50 ± 2.57%, N = 6 slices from 2 mice, $t_{(5)}$ = 9.549, $P < 0.001$; **Fig. 2**). H-6408 treatment significantly reduced this effect (–68.12 ± 6.79%, N = 13 slices from 4 mice, $t_{(12)}$ = 3.647, $P < 0.01$; electrical stimulation in H-6408: +16.38 ± 4.64%, $t_{(12)}$ = 3.526, $P < 0.01$; **Fig. 2b**,**d**) suggesting that most of the response to the stimulation was mediated by MCH.

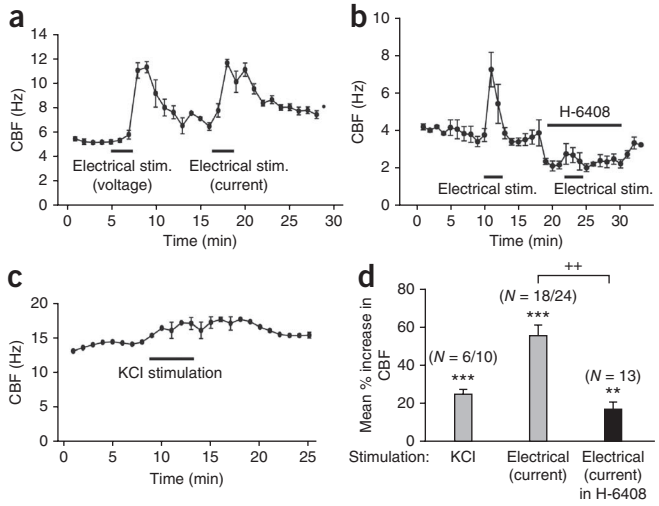

Figure 2 Stimulation of MCH neurons in brain slices increases CBF in neighboring ependymal cells along the v3V. (**a**–**c**) Stimulation by voltage or current (**a**,**b**) or by KCl (**c**) of fluorescent MCH neurons induced an increase in CBF in ipsilateral ependymal cells. The effect of stimulation was blocked by H-6408 (10 µM), which independently decreased the CBF (**b**). (**d**) Mean ± s.e.m. percentage increase in the CBF induced by KCl or electrical stimulation and its blockade by H-6408. The number of responsive slices/total number of slices are shown in parentheses. $^{**}P < 0.01$, $^{***}P < 0.001$, *t* test; ^{++}t = 142.5, U = 51.5, $P < 0.01$, Mann-Whitney test.

Our data indicate that MCH peptide increases the CBF in the v3V. A decrease in CBF is linked to an enlargement of the ventricles owing to a weaker evacuation and the progressive accumulation of CSF[4]. We first planned to assess the consequence of a systemic administration of an MCHR1 antagonist on CSF flow. However, the brain-penetrating MCHR1 antagonists that we used were only soluble in aprotic solvents (DMSO), and such a vehicle affected fluid dynamics in the brain (**Supplementary Fig. 6**), preventing pharmacological studies.

Using morphometric brain magnetic resonance imaging (MRI), we assessed ventricular volumes in wild-type (N = 3), $Mchr1^{+/-}$ (N = 5) and $Mchr1^{-/-}$ (N = 4) mice (**Fig. 3a**,**b** and **Supplementary Fig. 7**). LV volume, expressed as a percentage of total brain volume (**Fig. 3c**), was significantly greater in $Mchr1^{-/-}$ than in wild-type mice (wild type, 0.66 ± 0.10%; $Mchr1^{+/-}$, 1.03 ± 0.11%; $Mchr1^{-/-}$, 1.22 ± 0.15%; $H_{(2)}$ = 6.0256, $P < 0.05$, Kruskal-Wallis test; z = 2.3150, $P < 0.05$, Dunn's test for wild type versus $Mchr1^{-/-}$), as was the third ventricle volume (wild type, 0.39 ± 0.05%; $Mchr1^{+/-}$, 0.51 ± 0.01%; $Mchr1^{-/-}$, 0.55 ± 0.03%; $H_{(2)}$ = 6.7454, $P < 0.05$, Kruskal-Wallis test; z = 2.414445, $P < 0.05$, Dunn's test for wild type versus $Mchr1^{-/-}$; **Fig. 3d**). The fraction corresponding to the Sylvian aqueduct appeared to be reduced in $Mchr1^{-/-}$ mice (**Fig. 3e** and **Supplementary Fig. 7a**), although this was not statistically significant ($H_{(2)}$ = 5.6564, P = 0.0591,

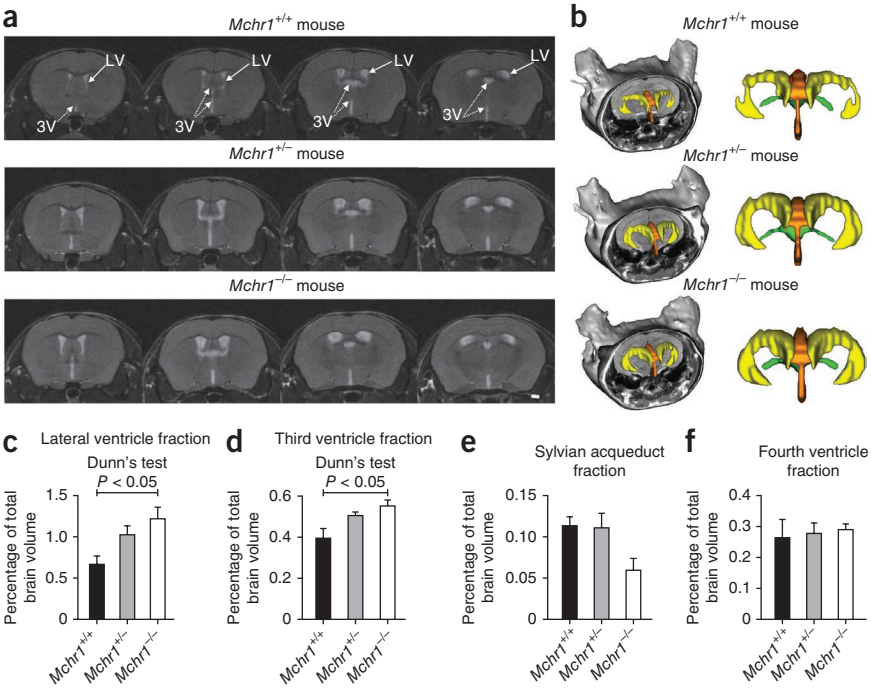

Figure 3 *In vivo* assessment of ventricle enlargement in *Mchr1*$^{-/-}$ mice. (**a**) Axial T_2-weighted brain images from wild-type (*Mchr1*$^{+/+}$), heterozygous (*Mchr1*$^{+/-}$) and *Mchr1*$^{-/-}$ mice at the level of the LVs and third ventricle. Scale bar, 1 mm. (**b**) Surface rendering of the ventricular system of *Mchr1*$^{+/+}$, *Mchr1*$^{+/-}$ and *Mchr1*$^{-/-}$ mice. First column: the ventricular system (LV and third ventricle) with the axial clipping plan. Second column: front view of the ventricular system. Yellow, LVs; orange, third ventricle; red, Sylvian aqueduct; green, fourth ventricle. (**c**–**f**) Volumetric analysis of ventricle size (means ± s.e.m).

Kruskal-Wallis test). The fourth ventricle fraction was similar in all groups ($H_{(2)} = 0.1385$, $P > 0.05$, Kruskal-Wallis test; **Fig. 3f** and **Supplementary Fig. 7a**).

Our results suggest a previously unknown role for the MCH system in regulating CSF flow and homeostasis via a specific CBF modulation of ependymal cells lining the v3V, but not d3V border. This spatial specificity adds a new level of complexity to the previously described characteristics of ciliated ependymal cells[3,7] and suggests that the CBF is fine-tuned in response to local changes in metabolic and neurohormonal molecules. Given that adjacent ciliated ependymal cells are coupled by gap junctions[8], the cluster-like distribution of MCHR1 along the v3V (confirmed in ref. 9) suggests that the few MCHR1-expressing cells may act as hubs and are responsible for the effect of MCH on the entire v3V epithelium[8]. MCH peptide likely activates MCHR1 at the basal pole of ependymal cells, where contacts with MCH fibers occur. However, as with other peptides, MCH is present in the CSF and may act through nonsynaptic mechanisms on MCHR1 at the apex of ciliated cells (**Fig. 1a** and **Supplementary Fig. 8**). Both ependymal cells and MCH neurons are involved in modulation of central glucose sensing[10–12]. Thus, it is possible that MCH fibers could control the activity of ciliated cells to initiate an increase in CSF flow to meet metabolic needs. Our MRI data revealed that ventricles upstream of the third ventricle were enlarged in *Mchr1*$^{-/-}$ mice, consistent with an alteration of CSF flow following dysfunction of ependymal cilia in the v3V[13,14]. Similarly, mouse models of Bardet-Biedl syndrome, a genetic disease caused by mutations in proteins involved in the trafficking of G protein–coupled receptors to primary cilia (including MCHR1)[15], show ventriculomegaly of the lateral and third ventricles[14]. Our data suggest that this may be partly a result of a defect in MCHR1 function in ependymal cells. In slices, H-6408 blocked the increase in CBF induced by both MCH and ipsilateral LHA stimulation. Given that the CBF is reduced to the same extent after H-6408 application and in *Mchr1*$^{-/-}$ mice, MCHR1 seems to exert a tonic positive effect on the CBF that is not compensated for during development. Brain-penetrating MCHR1 antagonists may thus alter CSF flow, limiting their potential use as therapeutic agents.

METHODS

Methods and any associated references are available in the online version of the paper.

Note: Supplementary information is available in the online version of the paper.

ACKNOWLEDGMENTS

We thank J.M. Friedman (Rockefeller University) for *Pmch-CFP* mice, J. Boutin (Institut de Recherche Servier) for the MCHR1 antagonists, F. Kober and T. Troalen for cine phase-contrast MRI tests, A. Le Troter for assistance in three-dimensional reconstruction of brain MRI, C. Houdayer for laser-capture dissections, V. Thieffin for animal care, I. Larre for help with immunoassays, F. Aguila for artwork, J. Chabry and P. Mollard for discussions, G. Agarwal for help with Matlab, and S. Rasika and P. Haghighi for corrections and remarks on the manuscript. Supported by the Agence Nationale de la Recherche (ANR; ANR-08-MNPS-018-01 to J.-L.N., ANR Gliodiabesity project to V.P. and ANR-09-BLAN-0267 to V.P.), the CNRS Institut National des Sciences Biologiques (INSB), European Union 6th Framework Program STREPS/NEST-APES 28594 (J.L.N.), Projets Exploratoires Premier Soutien (INSB; A.G. and J.-L.N.), the Fondation de la Recherche Médicale (J.-L.N.), and postdoctoral fellowships from the ANR-08-MNPS-018-01 and CNRS (INSB) and awards from the Société Française de Nutrition 2011 and the Institut Danone 2012 (G.C.). A.A. was supported by the Douglas Foundation, McGill University, Canadian Fund for Innovation, Research Chair (Tier 2), and Institute for Health Research and the Natural Science and Engineering Council of Canada.

AUTHOR CONTRIBUTIONS

G.C., F.B., A.V., F.L., B.D., V.P., L.L., C.R., P.M., S.H., P.-Y.R., A.P.-P. and A.G. performed the experiments. N.R. and O.M. engineered analytical tools. A.A. and B.L. engineered *Mchr1*$^{-/-}$ mice. G.C., A.V., V.P., T.L., R.C., P.-Y.R., J.-L.N. and A.G. analyzed the data. G.C., J.-L.N. and A.G. wrote the paper.

COMPETING FINANCIAL INTERESTS

The authors declare no competing financial interests.

1. Veening, J.G. & Barendregt, H.P. *Cerebrospinal Fluid Res.* **7**, 1 (2010).
2. Tissir, F. *et al. Nat. Neurosci.* **13**, 700–707 (2010).
3. Mirzadeh, Z., Han, Y.G., Soriano-Navarro, M., Garcia-Verdugo, J.M. & Alvarez-Buylla, A. *J. Neurosci.* **30**, 2600–2610 (2010).
4. Vígh, B. *et al. Histol. Histopathol.* **19**, 607–628 (2004).
5. Bittencourt, J.C. *et al. J. Comp. Neurol.* **319**, 218–245 (1992).
6. Hervieu, G. *Expert Opin. Ther. Targets* **7**, 495–511 (2003).
7. Nelson, D.J. & Wright, E.M. *J. Physiol. (Lond.)* **243**, 63–78 (1974).
8. Prochnow, N. & Dermietzel, R. *Histochem. Cell Biol.* **130**, 71–77 (2008).
9. Chee, M.J., Pissios, P. & Maratos-Flier, E. *J. Comp. Neurol.* **521**, 2208–2234 (2013).
10. García, M.A. *et al. J. Neurochem.* **86**, 709–724 (2003).
11. Psarra, A.M. *et al. J. Neurocytol.* **27**, 779–790 (1998).
12. Guyon, A. *et al. J. Neurosci.* **29**, 2528–2533 (2009).
13. Marshall, W.F. & Kintner, C. *Curr. Opin. Cell Biol.* **20**, 48–52 (2008).
14. Davis, R.E. *et al. Proc. Natl. Acad. Sci. USA* **104**, 19422–19427 (2007).
15. Berbari, N.F., Lewis, J.S., Bishop, G.A., Askwith, C.C. & Mykytyn, K. *Proc. Natl. Acad. Sci. USA* **105**, 4242–4246 (2008).

ONLINE METHODS

Animals and brain slices. All protocols were carried out in accordance with French ethical guidelines for laboratory animals (agreement N° 75-178, 05/16/2000) and approved by the Institut de Pharmacologie Moléculaire et Cellulaire Animal Care committee. Attention was paid to use only the number of mice requested and necessary to generate reproducible and reliable results.

Pmch-CFP transgenic mice (a kind gift of J.M. Friedman, Rockefeller University)[16], and wild-type and *Mchr1*$^{-/-}$ mice, all on the C57Bl6/J background, were obtained locally from heterozygous breeding pairs and were maintained on a 12-h dark/light cycle (7 a.m. to 7 p.m.) with food and water *ad libitum*. For fluorescent microscopy, electrophysiology, calcium imaging and CBF recordings, slices from 12–80-d-old males (N = 75 mice) were prepared as previously described[12], placed in a holding chamber (34 °C, 30 min) and then transferred to another incubation chamber at 22–25 °C, continuously perfused at a rate of 1–2 ml min^{-1} with gassed (95% O_2/5% CO_2) phosphate/bicarbonate-buffered saline (PBBS) containing 2 mM $CaCl_2$ (pH = 7.4), until recording. Drugs were applied to the slices through the perfusion system. All recordings were performed at 22–25 °C.

For immunohistochemistry, mice (N = 10) were anesthetized with isoflurane and perfused transcardially with saline, followed by a freshly prepared 4% paraformaldehyde (wt/vol) solution in phosphate-buffered saline (PBS, pH = 7.4). Brains were then post-fixed (paraformaldehyde, 12 h, 4 °C), cryoprotected (PBS/20% sucrose (wt/vol), overnight, 4 °C) and frozen until sectioning. *In vivo* brain MRI studies were performed on 4-month-old anesthetized female *Mchr1*$^{-/-}$ mice (three wild-type, five heterozygous and four *Mchr1*$^{-/-}$ mice).

Immunofluorescence. Coronal cryo-sections (20 µm thick, from three wild-type and three *Mchr1*$^{-/-}$ male mice to validate immunospecificity under our conditions and three *Pmch-CFP* mice; 3–4 sets of sections per mouse) were collected on chrome-alum-gelatin–coated slides. For each mouse, at least three independent sets of immunohistchemistry experiments were performed. Sections were then sequentially incubated in blocking solution (4% normal goat serum (vol/vol), 0.3% Triton X-100 (vol/vol) in PBS, 30 min, 22–25 °C), 0.1 M PBS (four times, 5 min, 22–25 °C), primary antibodies (in blocking solution, overnight, 4 °C), 0.1 M PBS (four times, 5 min, 22–25 °C) and a mix of secondary antibodies (1:500 in blocking solution, 1 h, 22–25 °C). Antibodies to MCHR1 (sc-5534, Santa Cruz Biotech)[17] and glu-tubulin[18] (AB3201, Millipore) were visualized using Alexa Fluor–conjugated secondary antibodies (Molecular Probes, Invitrogen). Antibody to vimentin[19] (AB5733, Millipore) was visualized using biotin-conjugated goat antibody to chicken (Vector Laboratories) and AMCA (amino-methylcoumarin acetate)-conjugated streptavidin (Vector Laboratories). Finally, sections were washed (four times, 5 min, 22–25 °C in 0.1 M phosphate buffer), coverslipped using Mowiol (Calbiochem) and stored at 4 °C until analysis.

Microscopic analysis. Sections were analyzed using an Axio Imager Z1 ApoTome microscope, equipped with a motorized stage and an AxioCam MRm camera (Carl Zeiss). Specific filter cubes were used for the visualization of green (excitation filter: 475/40 nm, dichroic mirror: 500 nm, emission filter: 530/50 nm), red (excitation filter: 550/25 nm, dichroic mirror: 570 nm, emission filter: 605/70 nm), and either ultraviolet (bisbenzimide) or AMCA fluorescence (excitation filter: 365 nm, dichroic mirror: 395 nm, emission filter: 445/50 nm). To create photomontages, single-plane images were captured using the MosaiX module of the AxioVision 4.6 system through a 20×/0.8 objective, sequentially for each fluorophore. Adobe Photoshop (Adobe Systems) was then used to process, by adjusting for brightness and contrast, and merge the photomontages. High-magnification photomicrographs represent maximal intensity projections derived from 20–25 triple ApoTome images collected using the z stack module of the AxioVision 4.6 system and a 63×/1.4 oil-immersion objective.

CBF measurements. CBF was extracted by image analysis using a high-speed complementary metal oxide semiconductor camera mounted on a bright-field video microscope. The fast Fourier transform (FFT) of the pixels was obtained from preprocessed and noise-reduced image sequences. This gave the power spectrum and the frequency, with the maximum amplitude indicating the CBF. As the FFT was not very effective over large volumes of data and yielded poor noise attenuation, a compressed spectrum was implemented. This Fourier-based technique was constructed using Matlab (7.10.0.499, R2010a release version) and used an average of the FFT of individual pixels. CBF measurement techniques are extensively described elsewhere (O.M., F.B. and A.G., http://hal.archives-ouvertes.fr/hal-00806681). In our conditions, the basal CBF varied from 2 to 27 Hz, with a mean of 11.18 ± 0.72 Hz (N = 55 slices in 14 mice). Slices showing basal CBF out of this range were excluded from analysis.

Stimulations of brain slices were carried out electrically with a bipolar electrode (at 1 Hz) or by perfusion with 135 mM KCl through a patch pipette placed close to the fluorescent cell bodies of MCH neurons in the hypothalamus of *Pmch-CFP* transgenic mice. We excluded from this set of data slices in which stimulation did not increase the CBF, possibly because the initial CBF was already too high (>16 Hz) or because the stimulated neurons did not project to the recorded area.

Electrophysiology. Slices were placed under an Axioskop upright microscope (Carl Zeiss) in a recording chamber superfused at a flow rate of 1 ml min^{-1} with oxygenated PBBS. Image acquisition was carried out with an AxioCam MRm infrared CCD camera controlled by Axiovison software (Carl Zeiss). Ciliated ependymal cells were patch clamped. Patch-clamp pipettes had a resistance of 4–7 MΩ when filled with the internal solution containing 120 mM KCl, 5 mM $MgCl_2$, 1 mM $CaCl_2$, 10 mM EGTA, 4 mM Na-ATP, 0.4 mM Na-GTP and 10 mM HEPES (pH adjusted to 7.3 with KOH). Current-clamp experiments were performed with a potassium gluconate solution containing 130 mM potassium gluconate, 1 mM $MgCl_2$, 0.3 mM $CaCl_2$, 1 mM EGTA, 4 mM Mg_2ATP, 0.4 mM Na_3GTP and 10 mM HEPES. Input resistance varied between 12 and 20 MΩ and was left uncompensated. Measurements started 2–3 min after obtaining the whole cell to ensure dialysis of the intracellular medium. Data were digitized at 5–10 kHz with a Digidata interface coupled to a computer running pClamp 9 (Axon Instruments).

Fura-2AM experiments. The $[Ca^{2+}]_i$ was measured in slices using the membrane-permeable acetoxymethyl fura-2 ester (Fura-2AM, Invitrogen) dissolved in DMSO. Slices were incubated for 40 min in a Petri dish filled with PBBS supplemented with 10 µM Fura-2AM + 0.04% pluronic acid (vol/vol), gassed with 95% O_2/5% CO_2, then washed in PBBS for 15 min. Fura-2AM–loaded slices were transferred to a continuously perfused (1 ml min^{-1}) recording chamber on an inverted-fluorescence microscope (AxioObserver, Carl Zeiss) equipped with a Xenon 300-W illumination source (Lambda LS, Sutter Instruments). $[Ca^{2+}]_i$ changes were imaged with a Fluar 40×/1.3 oil-immersion objective at 22–23 °C. The intracellular Fura-2AM was sequentially excited at 340 and 380 nm through a high-speed multi-filter wheel and, for each excitation, a fluorescence emission image was obtained through the same 400 LP dichroic mirror and 510BP40 filter. Fluorescence images were acquired for an exposure time of 100 ms with a cooled black and white Cascade 512B EMCCD camera (Photometrics, Roper Scientific), every 5 or 2 s. All equipment was controlled by MetaFluor software (Molecular Devices, Roper Scientific). Background was subtracted from fluorescence images. The $[Ca^{2+}]_i$ in identified Fura-2AM–loaded ependymal cells was estimated as a function of time by using fluorescence ratio (R = F340/380).

***In vivo* brain MRI.** Mice were imaged at high field using an 11.75-T vertical Bruker AVANCE 500 WB wide-bore MRI system (Bruker) with a transmitting and receiving head resonator of 2.5 mm. Mice were anesthetized with an intraperitoneal injection of ketamine (100 mg per kg of body weight) and xylazine (10 mg per kg), and placed in a cradle equipped with a stereotaxic holder and a pressure probe to monitor the respiratory rate. Body temperature was maintained at 37 °C using the magnet gradients. T_2-weighted images were acquired in the axial plane using a spin-echo sequence (echo time = 37.1 ms, repetition time = 5,000 ms, rapid acquisition with a relaxation enhancement factor of 8, 4 averages). Geometric variables for T_2-weighted images were as follows: 30 contiguous 0.5-mm-thick slices, matrix of 256^2 and field of view of 400 mm^2, leading to an in plane resolution of 78 µm and a pixel size of 6.1 ×10^{-3} mm^2. MRI data were processed using DISPIMAG, homemade software developed under the IDL environment (Interactive Data Language Research System). Brain and ventricle volumes were calculated using a function provided by IDL, which finds regions of similar amplitude. The volume of a selected ventricle was expressed as a percentage of brain volume to take into account inter-individual variations in head size among mice[20]. The three-dimensional reconstruction of the ventricular system was obtained using the BrainVisa software (http://brainvisa.info/).

doi:10.1038/nn.3401

Drugs. 5-HT and ATP were obtained from Sigma-Aldrich, and MCH and H-6408 were from Bachem. J. Boutin (IdRS) kindly provided us with MCHR1 antagonists, including DIVO1974. All drugs were prepared as stock solutions in water, frozen and then diluted to their final concentration before use, except for DIVO1974, which was dissolved in DMSO.

Statistics. The statistical significance of differences between groups (data expressed as means ± s.e.m.) was tested using unpaired Student's *t* test or, when the values were not following a normal distribution, the non-parametric Mann-Whitney test. Degrees of freedom are given in parentheses. Statistical analysis was carried out using SigmaPlot (Jandel) and Origin (Microcal) software. For brain MRI, because of the small size of the groups (wild-type, $N = 3$ mice; *Mchr1*$^{+/-}$, $N = 5$, *Mchr1*$^{-/-}$, $N = 4$), we used the non-parametric Kruskal-Wallis test followed by a *post hoc* Dunn's multiple comparison test (Prism 5.0a software, GraphPad software) to compare the three groups of mice. $P < 0.05$ was considered to be significant.

16. Stanley, S. *et al. Proc. Natl. Acad. Sci. USA* **107**, 7024–7029 (2010).
17. Berbari, N.F., Johnson, A.D., Lewis, J.S., Askwith, C.C. & Mykytyn, K. *Mol. Biol. Cell* **19**, 1540–1547 (2008).
18. Paturle-Lafanechère, L. *et al. J. Cell Sci.* **107**, 1529–1543 (1994).
19. Prevot, V. *J. Neuroendocrinol.* **14**, 247–255 (2002).
20. Penet, M.F. *et al. Behav. Genet.* **36**, 732–744 (2006).